The Characteristics of Summer Heavy Rains from Atmospheric River Related to Low Level Jets & Typhoons, MJO & ENSO, and Monsoon

Okjin Jung 01, Yun-Seob Moon* 02, Da Bin Kim 02, Cheol-Jae Lee 03

01 Chungbuk Carbon Neutrality Center

02 Department of Environment Education, Korea National University of Education

03 Kangwon Taebak Elementary School

Abstract

Given the increasing severity of summer heavy rains on the Korean Peninsula, identifying their causes is essential for preparing for abnormal weather patterns. This study aims to analyze the relationship between temporal variations in Total Precipitable Water (TPW) and atmospheric fluctuations such as low-level jets, typhoons, the Madden-Julian Oscillation (MJO), the El Niño-Southern Oscillation (ENSO), and the monsoon to clarify the causes of summer heavy rains that have occurred on the Korean Peninsula in East Asia from 2018 to 2019. To achieve this, the study employs a combination of observational data and meteorological reanalysis to investigate the relationship between TPW and the identified atmospheric fluctuations. The data sources include satellite measurements, ground-based observations, and global reanalysis datasets. The analysis of the spatial distribution of TPW revealed that water vapor concentrated in the Western Pacific near the thermal equator influenced the occurrence and movement of typhoons, which in turn affected precipitation on the Korean Peninsula. Specifically, during the case study days: In the first instance, TPW was influenced by a tropical depression located in the east longitude zone near the thermal equator, passing along the western coast of the Korean Peninsula. In the second instance, TPW was affected by a tropical depression situated in the east longitude zone, directly passing through the Korean Peninsula. In the third instance, TPW was influenced by a tropical depression positioned in the east longitude zone, located east of the Korean Peninsula. These findings indicate the significant role of tropical depressions in determining the TPW distribution and subsequent heavy rainfall events on the Korean Peninsula.

Key words: total precipitable water, atmospheric river, frontogenesis, Rossby wave, tropical cyclones

I. Introduction

In recent years, the Korean Peninsula has experienced an increase in the frequency and intensity of summer heavy rainfall, causing significant socio-economic damage. These extreme weather events are closely related to the climate crisis, necessitating an understanding and preparedness through the analysis of interactions with various atmospheric phenomena. Summer heavy rainfall is primarily driven by high moisture content in the atmosphere and the meteorological conditions that facilitate it. Existing studies have identified key factors such as Atmospheric Rivers (ARs), low-level jets, typhoons, the Madden-Julian Oscillation (MJO), the El Niño-Southern Oscillation (ENSO), and monsoons.

Total Precipitable Water (TPW) data, which represents the total atmospheric water vapor globally, reveals moisture flows extending from mid-latitudes towards the poles, resembling rivers, hence termed Atmospheric Rivers (ARs)

(Gimeno et al., 2014; Dacre et al., 2015). ARs are characterized by narrow and elongated bands of strong moisture transport, primarily occurring in the warm sector of mid-latitude cyclones and accounting for most moisture transport from mid-latitudes to the poles (Zhu and Newell, 1994; Neiman et al., 2008; Moon et al., 2019). The formation of ARs begins with strong winds over moisture-rich seas, transferring moisture to the atmosphere, which is then transported by low-level jets. These jets, defined as strong wind bands blowing at 25 kt (12.5 m/s) or more at 700–850 hPa during summer, play a crucial role in moisture transport, horizontal divergence, and the formation of upward motion (Chen et al., 1988; Park et al., 2003).

The summer heavy rainfall patterns in the Northern Hemisphere are closely related to ARs. ARs are also closely associated with other phenomena such as low-level jets, typhoons, MJO, ENSO, and monsoons.

Typhoons, with their strong winds and abundant moisture, significantly contribute to heavy rainfall, with their paths and intensities influenced by factors such as sea surface temperature, the beta effect, and surrounding steering flows (Kim et al., 2021; Seo et al., 2017). MJO, a large-scale atmospheric circulation and deep convection phenomenon in tropical regions, is associated with Rossby waves that propagate to mid-latitudes, transporting substantial amounts of moisture to continents via ARs, potentially causing heavy rainfall (Seo et al., 2017; Kim et al., 2008). ENSO impacts atmospheric circulation patterns during El Niño and La Niña periods, altering heavy rainfall patterns (Wang and Lin, 2002; Wang et al., 2003; Xie et al., 2009). Monsoons, driven by the difference in heat capacity between land and sea, lead to seasonal changes in wind direction, with the summer southwest monsoon and East Asian monsoon transporting large amounts of moisture to the atmosphere, causing heavy rainfall (An et al., 2015; Kim et al., 2016).

This study investigates the relationship between TPW and various atmospheric variations using observational data and weather reanalysis data from cases of heavy rainfall in the Korean Peninsula during 2018 and 2019. By analyzing the spatial distribution of TPW and its correlation with atmospheric variations, this research seeks to clarify the main causes of heavy rainfall and contribute to the development of effective disaster response strategies based on these findings. The insights gained from this research are expected to enhance predictive capabilities and preparedness strategies in the face of ongoing climate change, ultimately contributing to more robust climate resilience.

II. Data and Analysis Methods

1. IWV and IVT

IWV, short for Integrated Water Vapor, refers to the total amount of water vapor contained in a column of air from the surface to the top of the atmosphere, assuming a column with an area of 1 m² on the surface (unit: kg/m² = 0.1 g/m² = mm). Similar to TPW, IWV is used as an indicator of atmospheric moisture content and is utilized as a measure of the amount of water vapor within the air column. Atmospheric rivers are defined as when the value exceeds 20, indicating a state of strong moisture transport (Ralph et al., 2004). IWV is defined as:

$$\mathbf{TPW} = \mathbf{IWV} = \int_{z=0}^{z=\infty} \rho q dz = \frac{1}{g}\int_{p=0}^{p=p_{sfc}} q dp$$

where ρ is the air density, q the specific humidity, z the altitude, g the gravitational acceleration, p the pressure, and

p_{sfc} the surface pressure.

The moisture transport between each isobaric surface in the atmosphere is expressed in the form of water vapor (horizontal) flux. When the vertically integrated water vapor flux is greater than 250 kg/m/s, it is referred to as an Atmospheric River (Rutz et al., 2014). The formula is as follows:

$$\mathbf{IVT} = (\boldsymbol{IVT_u}, IVT_v) = \frac{1}{g}\int_{\mathbf{0}}^{\boldsymbol{p_{sfc}}} [\boldsymbol{u}, \boldsymbol{v}]\boldsymbol{qdp}$$

where u is the wind speed in the east-west direction, and v the wind speed in the north-south direction. For example, the vertically integrated water vapor flux (IVT) from the sea surface to the 500 hPa level is the total amount of water vapor passing through a surface with a width of 1 meter per second and extending to the height corresponding to the 500 hPa level in one second.

2. The Impact of Typhoon Position or the Asian Summer Monsoon on Precipitation

Understanding the impact of typhoon position or the Asian summer monsoon on precipitation, we analyzed the distribution of Velocity Potential (VP, $10^6 m^2/s$) anomalies at the 200 hPa level. Velocity Potential is calculated from the non-divergent (divergent component) velocity in a two-dimensional flow. Two-dimensional flow is categorized into non-divergent wind (rotational component) and divergent wind (non-rotational component), the former is the stream function (Ψ, m^2/s) and the latter is the derivative of speed potential (φ, m^2/s). The formula is as follows:

$$v = v_\psi + v_\chi$$

$$v_\psi = k \times \nabla\psi$$

$$u_\psi = -\frac{\partial\psi}{\partial y}$$

$$v_\psi = -\frac{\partial\psi}{\partial x}$$

$$\zeta = \frac{\partial v}{\partial x} - \frac{\partial u}{\partial y} = \nabla^2\psi = \frac{\partial^2\psi}{\partial x^2} + \frac{\partial^2\psi}{\partial x^2}$$

$$v_x = \nabla x = \frac{\partial\chi}{\partial x} + \frac{\partial\chi}{\partial y}$$

$$u_\chi = -\frac{\partial\chi}{\partial x}$$

$$v_\chi = -\frac{\partial\chi}{\partial y}$$

$$\text{div } v_\chi = \nabla^2\chi = \frac{\partial u}{\partial x} + \frac{\partial v}{\partial y}$$

approximately, the geostrophic wind corresponds to v_ψ since it assumes non-divergent wind (f is assumed to be a constant), and the contours correspond approximately to ψ.

III. Results

1. Characteristics of Summer Heavy Rainfall Associated with ARs

Atmospheric Rivers (ARs) are narrow regions where large amounts of water vapor are transported from the equator to mid-latitudes or high latitudes. This term refers to the total precipitable water vapor flowing like a river. Specifically, in Figures 1 to 3, ARs are depicted as band-shaped streams 300 to 500 km wide with total precipitable water exceeding 20 mm (Ralph et al., 2004). The flow of these ARs is directly related not only to heavy summer rainfall on the Korean Peninsula but also to global summer heavy rainfall and winter snowstorms (Gimeno et al., 2014). According to the Korea Meteorological Administration (www.kma.go.kr), when TPW exceeds 25 mm, there is a high likelihood of showers and thunderstorms occurring. TPW is influenced by the evaporation of water from the surface, precipitation in the atmosphere, and the movement of water vapor by horizontal winds.

Figures 1 to 3 show the spatial distribution of TPW for cases of heavy rainfall that occurred on the Korean Peninsula in 2018 and 2019. During these events, TPW exceeding 50 mm was observed in the summer due to the influence of ARs. Additionally, the accumulated precipitation on radar composite photographs exceeded 5 mm, with heavy rainfall mainly occurring in the southern regions of the Korean Peninsula (Figure 4).

Figure 1 shows the global distribution of TPW from August 21 to 22, 2019. Observing the distribution where TPW exceeds 20 mm, it is evident that water vapor from near the equator is transported to higher latitudes through the mid-latitudes. In the Northern Hemisphere, a band of water vapor with a width of 300 to 500 km originates from near the thermal equator in the western Pacific, moving northeastward along the East China Sea, passing through Korea, and continuing across Japan and the Pacific, reaching the coast of Alaska and North America, indicating a giant atmospheric river. Additionally, one stream originating from the thermal equator between the eastern Pacific and western Atlantic is found to connect to the Arctic through the UK and Europe. In contrast, the Southern Hemisphere shows about six atmospheric river streams heading toward Antarctica in a comma-shaped pattern. When these ARs pass over continents or islands during the summer, continuous air mass uplift leads to heavy rainfall in those regions. Conversely, in winter, this leads to heavy snowfall. The spatial distribution of TPW in mid-August 2019 indicates strong activity near the Indian monsoon region, the thermal equator region of the western Pacific, the thermal equator region between the eastern Pacific and western Atlantic, and near the thermal equator region of West Africa. These features are related to the high heat capacity (or specific heat) of the thermal equator regions of the continents during summer and are associated with phenomena such as monsoons, MJO, and ENSO. Furthermore, ARs are linked with typhoons from TPW nuclei exceeding 70 mm near the thermal equator, and the regular comma-shaped pattern of ARs in the Southern Hemisphere and the comma-shaped low-pressure systems in the mid-latitudes of the Northern Hemisphere indicate that ARs are connected to mid-latitude cyclones' fronts. The relationship between TPW and these phenomena will be discussed in the next section.

Figure 2 shows the global distribution of TPW from August 24 to 27 and September 2 to 3, 2018. A large band-shaped TPW exceeding 50 mm near the thermal equator in Southeast Asia enters Japan and the Korean Peninsula through the East China Sea, forming a broad and extensive AR that reaches North America via the North Pacific. During this time, Korea experienced heavy rainfall in the form of a monsoon front from August 23 to 27. A similar AR, though weaker in intensity, was observed along the Atlantic in the thermal equator seas of the Americas (Figure 2(a)). The AR in the western

Pacific of the Northern Hemisphere started from a cyclone or typhoon with TPW exceeding 70 mm in the thermal equatorial region of Southeast Asia and moved northeastward, connecting with mid-latitude cyclones and reaching North America. In the case of Korea, Typhoon Cimaron moved northeastward through the East China Sea, supplying a large amount of water vapor to the Korean Peninsula. Meanwhile, six days later, on September 2 and 3, another typhoon, Soulik, approached, reinforcing the existing AR over Korea in the form of a monsoon front due to the influence of warm and humid air masses from the south. As Typhoon Soulik transformed into a mid-latitude cyclone, the AR broadened and continued to affect North America.

Figure 3 shows the spatial distribution of TPW in the northwestern Pacific on September 21, 2019, forming an AR under the influence of a typhoon. This is a case where water vapor was introduced to the Korean Peninsula due to Typhoon Tapah, with TPW nuclei exceeding 70 mm. Including Typhoon Tapah, a group of four typhoons connected with mid-latitude cyclones to form one AR, which moved toward North America.

Figure 4 shows the accumulated precipitation on radar composite images over the Korean Peninsula on August 21-22 and September 21, 2019. This distribution represents the accumulated precipitation when the atmospheric river of TPW mainly passed through the southern region of the Korean Peninsula. During this time, the southern region experienced heavy rainfall with rates exceeding 10 mm per hour in a northeast-southwest direction.

Consequently, it can be observed that the ARs of TPW act as narrow and strong flows transporting water vapor from near the thermal equator towards the mid-latitudes, directly affecting the flow of water vapor over the Korean Peninsula and contributing to heavy summer rainfall. Particularly, the occurrence of typhoons near the thermal equator gathers water vapor in the western Pacific, forming an atmospheric river connected to mid-latitude cyclones towards East Asia or moving as a typhoon itself, influencing precipitation. The ARs or typhoons affecting the Korean Peninsula subsequently impacted North America by following the fronts of mid-latitude cyclones as part of a large AR. Additionally, the spatial distribution characteristics of TPW gather in high heat capacity thermal equator regions of continents during summer, which is associated with phenomena such as monsoons, the MJO, and ENSO.

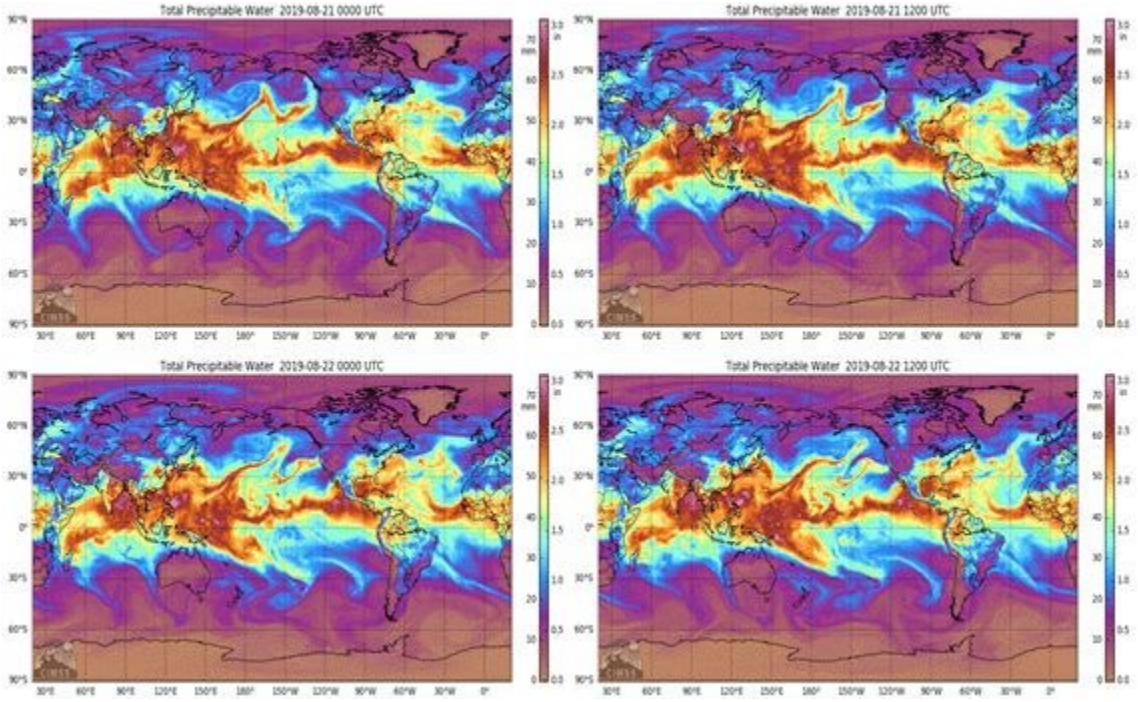

Figure 1. Spatial distribution of total precipitable water(mm) for the period from 21 to 22 August 2019.

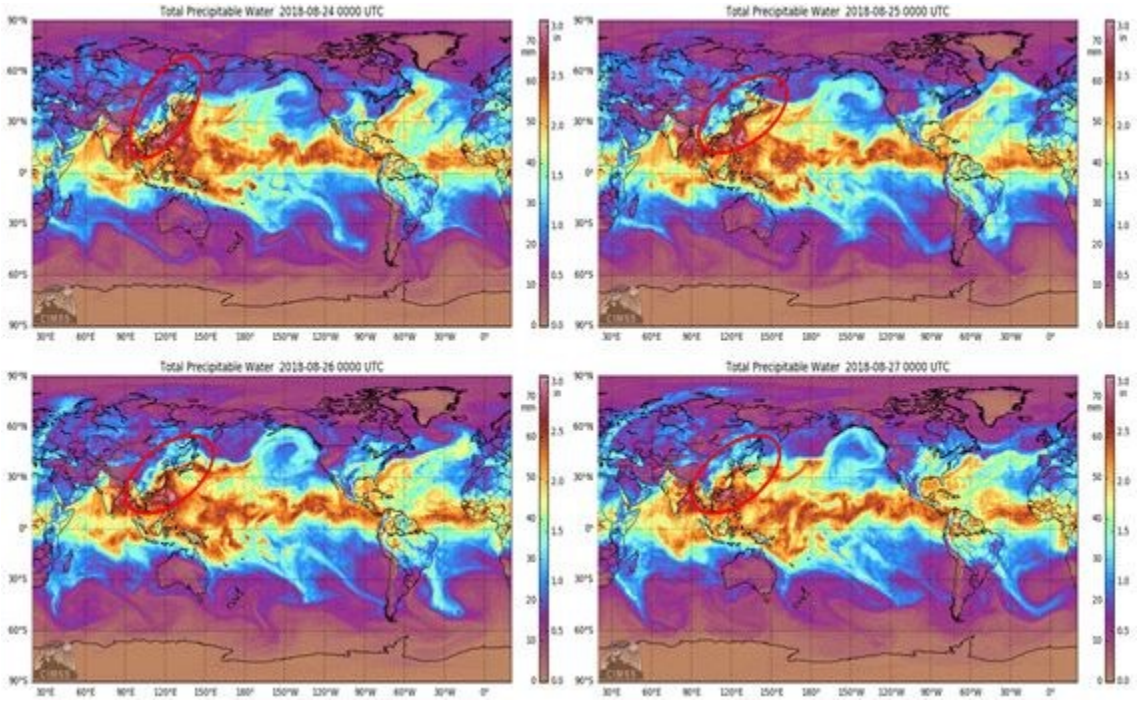

(a)

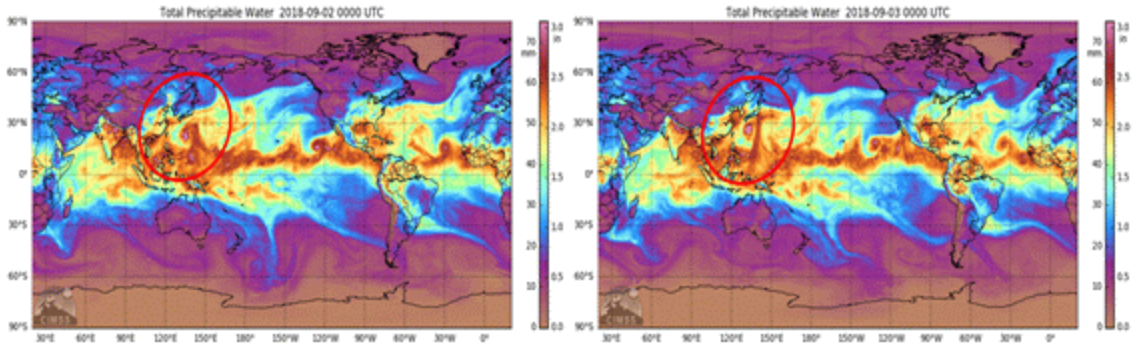

(b)

Figure 2. Spatial distribution of total precipitable water(mm) for the periods (a) from 24 to 27 August 2018 and (b) from 2 to 3 September 2018.

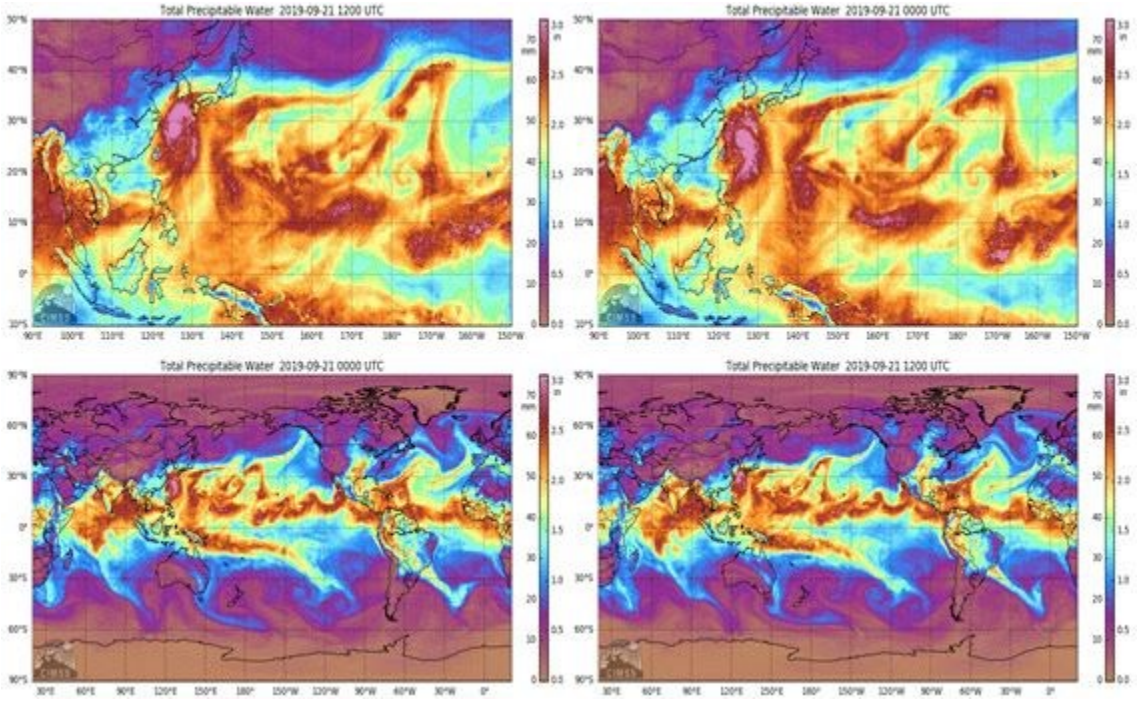

Figure 3. Spatial distribution of total precipitable water(mm) in the West Pacific and global area for the period from 21 to 22 September 2019.

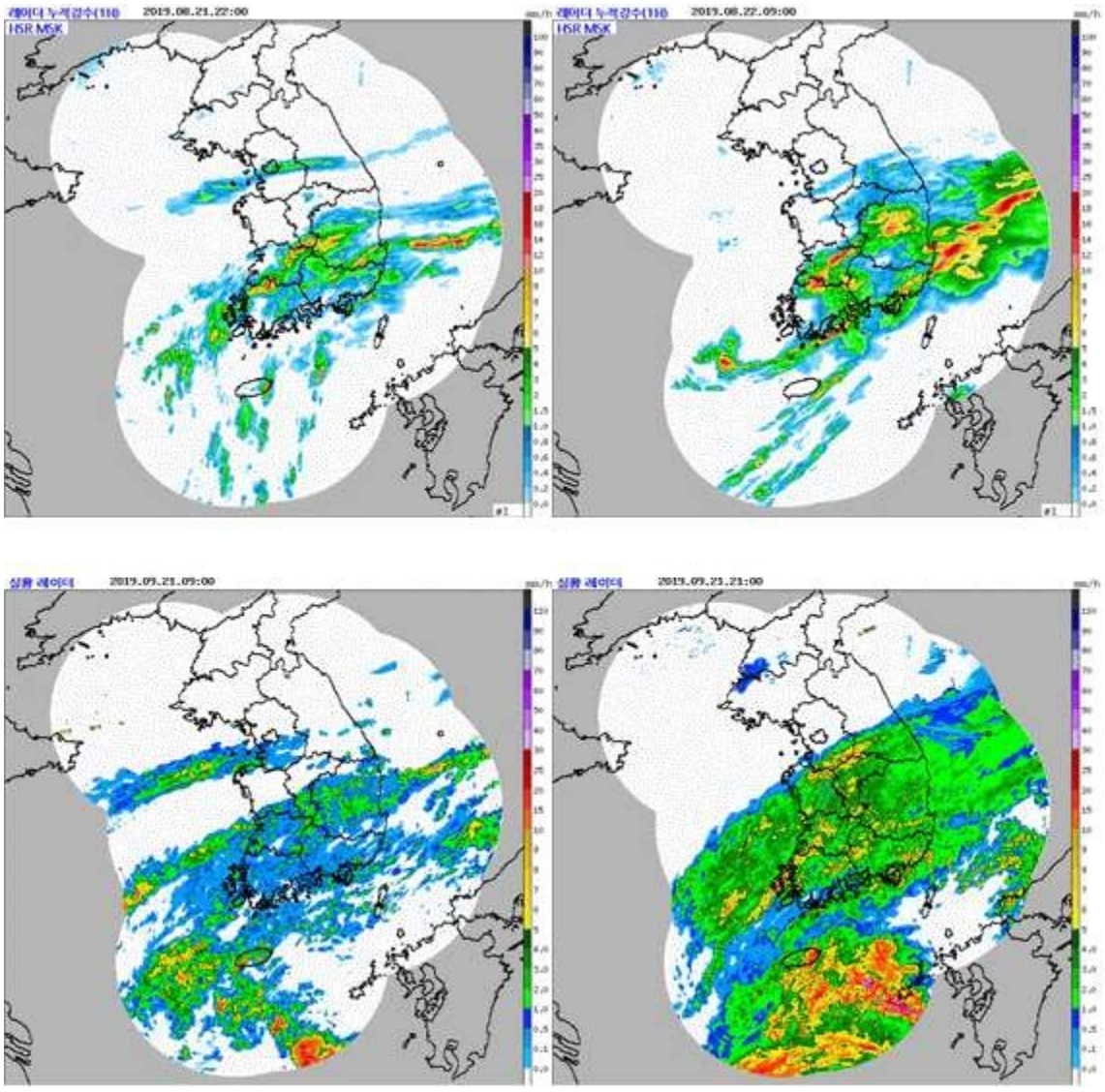

Figure 4. Radar composite photographs of precipitation(mm) (a) for the period from 21 to 22 August 2019 and (b) on 21 September 2019.

2. Transport of TPW by Low-Level Jets and Typhoons

By analyzing the TPW depicted in Figures 1 to 3, we can understand the causes of the record-breaking heavy rainfall (approximately 300mm per hour) in the central or southern regions of the Korean Peninsula since 2017. This is primarily due to the movement of typhoons and the flow of moisture from the Chinese continent or subtropical regions, forming a monsoon front over the central or southern Korean Peninsula, leading to heavy rainfall. Apart from typhoons, what drives this AR (Atmospheric River), i.e., the transport of total moisture?

According to Ralph et al. (2004, 2006), a typical AR creates a concentrated band of enhanced moisture along the warm conveyor belt in the frontal region of a mid-latitude cyclone's cold front, causing vertical uplift through the convergence of air. This process generates a low-level jet resulting from the temperature gradient across the cold front. Consequently,

the transport of ARs is locally converged along the cold front of mid-latitude cyclones or originates from the direct poleward movement of tropical moisture (Bao et al., 2006).

Figures 5 and 6 show the spatial distribution on August 21 and September 21, 2019, respectively, of temperature (°C), streamlines (m^2/s), and wind vectors (m/s) at an altitude of 10 km; potential velocity divergence (10^6 m^2/s) and isotachs (dashed lines, $\geq$50 knots) at the 200 hPa level; and geopotential height (m), temperature (°C), and mixing ratio (g/kg) at the 850 hPa level.

As shown in Figures 1 to 3, transporting TPW from the Indian monsoon region and the western Pacific thermal equator to the atmosphere over the Korean Peninsula is only possible through strong winds or typhoons. The cases from August 21 to 22, 2019, in Figure 1, and August 24 to 27 and September 2 to 3, 2018, in Figure 2, although occurring in different periods, illustrate that strong winds associated with typhoons, namely low-level jets, brought TPW into the Korean Peninsula. This resulted in primary rainfall with the first front, which was subsequently enhanced by the following typhoon, leading to secondary rainfall, or the typhoon itself directly approached, causing tertiary rainfall. The case from September 21 to 22, 2019, in Figure 3, is a typical example where TPW was directly introduced to the Korean Peninsula by the typhoon itself. In the former cases, the occurrence and northward movement of typhoons from the Indian monsoon region and the Philippine thermal equator region play a crucial role in transporting TPW to the Korean Peninsula.

The regions where typhoons occur can be identified by the central pressure distribution in meteorological satellite images or surface weather maps. However, as mentioned in the previous section, the location of a typhoon can be identified by the appearance of TPW nuclei exceeding 70 mm. Another method to determine the location of a typhoon is by identifying areas with low vertical wind shear in the atmosphere, which can also be seen through the distribution of velocity potential anomalies at the 200 hPa level. It is known that typhoons occur in regions with positive values of upper-level divergence in the oceanic areas near the thermal equator, as indicated by 200 hPa velocity potential anomalies (Higgins and Shi, 2001). According to existing research, typhoons tend to form in regions with high temperature and humidity where the northeast trade winds and southeast trade winds converge, particularly during July to September when the thermal equator, or Intertropical Convergence Zone (ITCZ), moves northward away from the equator. Additionally, it has been noted that typhoons frequently form in the summer monsoon trough (MT), where the ITCZ and counterclockwise monsoon circulation meet. This occurs as the monsoon trough moves northward to around 20°N at the northern tip of the Indochina Peninsula and extends to the ITCZ east of the Philippines.

In Figures 5(a) and 6(a), the location of tropical cyclones can be identified by the counterclockwise concentric wind vectors in the northwest Pacific. Whether these tropical cyclones are typhoons can be verified by checking if they correspond with regions of positive velocity potential anomalies at the 200 hPa level, as shown in Figures 5(c) and 6(c). On August 21, 2019, one typhoon was located in the Japanese mainland southeast of Korea, and one each southwest of Taiwan and south of the Philippines. These typhoons align with the TPW nuclei exceeding 70 mm seen in Figures 1 to 3. Additionally, the formation locations of these typhoons in the examples from Figures 1 and 2 correspond to the Monsoon Trough (MT) moving northward to the northern tip of the Indochina Peninsula and extending to the ITCZ east of the Philippines.

Figures 5(b) and 5(d) and Figures 6(b) and 6(d) show the streamlines and mixing ratio at the 850 hPa level, indicating the TPW transport paths via strong winds or low-level jets. Figures 5(a) and 6(a) illustrate the TPW transport routes at the surface through wind patterns along with front formation. In Figures 5(a) and 6(a), wind vectors at an altitude of 10 km show fronts forming where cold northern air meets warm southern air. Comparing these fronts with the streamlines at the 850 hPa level in Figures 5(b) and 6(b) reveals a prominent streamline directed towards the Korean Peninsula, indicating that the TPW mixing ratio forms an atmospheric river along these fronts and streamlines. These results demonstrate that atmospheric rivers are formed by TPW along the fronts of large-scale north-south flows influenced by strong winds (low-level jets) or typhoons.

In the cases shown in Figures 1 and 2, as typhoons move northward, the pressure systems ahead often slow down or become stationary (blocking). Discontinuities form along the northern boundaries of the warm, humid air masses brought by typhoons, creating rain bands and sometimes strengthening weakened fronts (Lee, 2006). The front ahead of the typhoon acts as an obstacle, affecting the typhoon's speed. An example from August 2018 showed Typhoon Cimaron moving northward between Typhoon Soulik and a subtropical high, slowing Soulik's movement to below 10 knots (Kim et al., 2021). In such cases, TPW linked to mid-latitude cyclones via low-level jets causes initial heavy rainfall in the southern regions, and as the typhoon approaches Korea, it strengthens the first front, leading to secondary heavy rainfall in the central or northern regions. The third phase involves the typhoon itself causing strong winds and heavy rain based on its central pressure and water vapor content.

Thus, atmospheric rivers heading towards Korea (TPW ≥ 20 mm) are initially influenced by typhoons and typically follow strong low-level jet streams, i.e., along fronts at the 850 hPa level where cold northern air meets warm southern air. The TPW forms a warm conveyor belt along the fronts, causing rainfall initially in the southern regions. The advancing typhoon then strengthens this front, acting as a blocking system, slowing the typhoon and moving the front northward, causing rainfall in the central and northern regions. As the typhoon makes landfall, it brings strong winds and heavy rain. Another scenario involves direct TPW inflow from a typhoon moving towards Korea. Ultimately, it is evident that atmospheric rivers are formed by TPW along the fronts of large-scale north-south flows, influenced by strong winds (low-level jets) or typhoons.

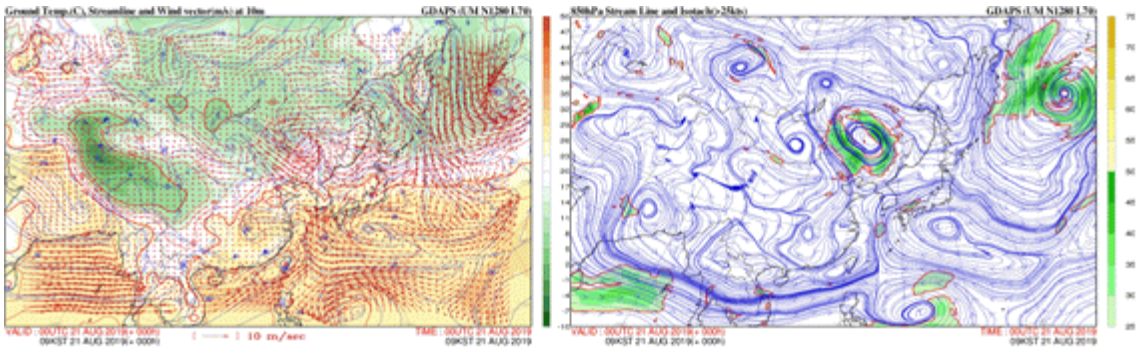

(a) (b)

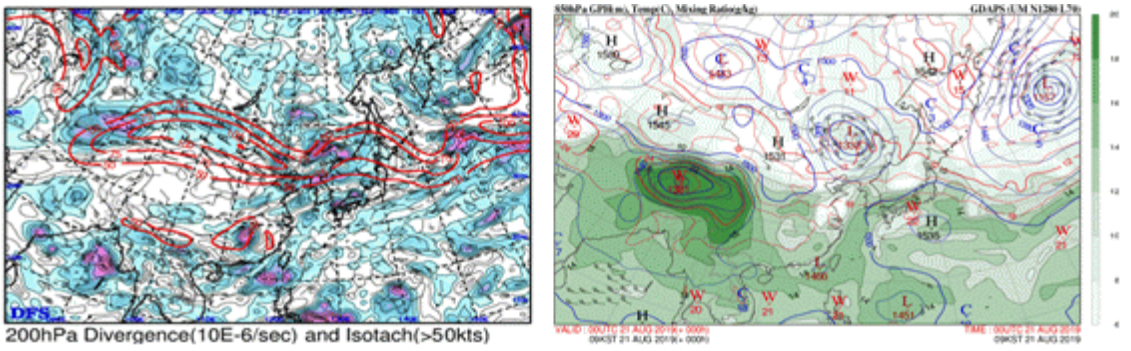

(c) (d)

Figure 5. Spatial distribution of (a) ground air temperature(℃), streamline(m^2/s), and wind vectors(m/s) at 10m , (b) stream line and isotach(color shaded, ≥25 knots), (c) 200hPa divergence(10^6 m^2/s) and isotach(thic lines, ≥50 knots), (d) 850hPa GPH(m), air temperature(℃), mixing ratio(g/kg) at 0000UTC on 21 August 2019.

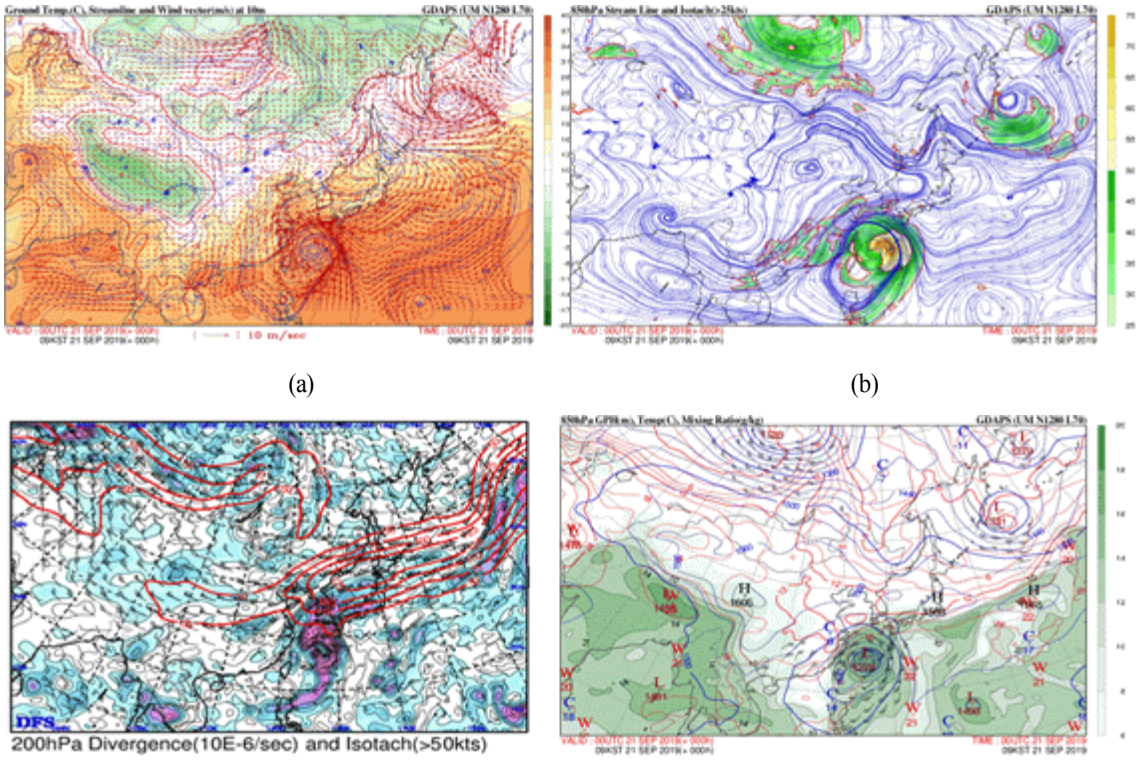

(a) (b)

(c) (d)

Figure 6. Same as except for on 21 September 2019.

3. TPW Changes Related to MJO, ENSO, and Monsoons

In Figures 1 to 3, the global distribution of TPW illustrates that the spatial distribution of TPW is related to phenomena such as typhoons, the MJO, the ENSO, and monsoons. In August 2018 and 2019, TPW was concentrated in the Indian

monsoon region and the Philippine seas, coinciding with the convective region of the MJO in these areas. As mentioned in the introduction, typhoons forming along this thermal equator increase vorticity related to the monsoon, propagating northward along Rossby waves towards Korea or Japan (Kim et al., 2008; Kim and Seo, 2016). This can be observed in Figures 1 to 3 and Figure 5.

The deep convective regions of the MJO and the probability of typhoon formation can be identified through relative vorticity anomalies at 850 hPa, OLR, areas of low vertical wind shear, or the velocity potential anomaly distribution at 200 hPa (Kim, 2011). The distribution of 200 hPa divergence winds and velocity potential anomalies can indicate the location of typhoons and the rainfall regions of the Asian summer monsoon. MJO deep convection is typically indicated by OLR anomalies, where deep convection leading to high cloud tops results in negative OLR anomalies due to less longwave radiation being emitted, while regions without convection exhibit positive OLR anomalies. The presence of El Niño can be determined by sea surface pressure or SST anomalies in warm pool and cold tongue regions, or by positive values of the Southern Oscillation Index (SOI), indicating positive sea surface pressure anomalies in the equatorial eastern Pacific (Deser et al., 2010).

This study investigates the relationship between TPW distribution from August 24-27 and September 2-3, 2018 (Figure 2), and phenomena such as MJO, ENSO, and monsoons, including the position of typhoons. Figure 7 depicts 850 hPa wind vector anomalies from August 22 to 31, 2018, during which the convective region of the MJO was located in the Indian monsoon region. From August 22 to 26, positive wind vector anomalies (westerlies) extended from the monsoon region across the Indochina Peninsula and the eastern seas of the Philippines, following the South China Sea to Korea and Japan, continuing to propagate as Rossby waves towards North America, with TPW distributed in AR form along these wind bands. From August 27 to 31, the westerly distribution, indicated by positive wind vector anomalies, narrowed due to strengthened trade winds (negative anomalies) in the western Pacific, propagating towards Korea through the South China Sea, China, and Japan in the form of Rossby waves. This period from August 22 to 31, 2018, saw the Rossby waves dominating along the Pacific edge, starting from the Indian monsoon region, spreading through the Philippines, South China Sea, Korea, Japan, and North America, with TPW distributed along these bands.

Figure 8 shows OLR anomalies from July 25 to August 23, 2018, where blue circles and shading represent negative anomalies indicating wetter conditions or convection, while red circles and shading represent positive anomalies indicating drier conditions. In late July and early August, widespread enhanced convection was observed in the northwest Pacific, covering the western Indian Ocean, South Asia, and the equatorial western Pacific. OLR fields became more complex in early August, with enhanced convection concentrating across the western Pacific and extending to the Indian-Southeast Asian monsoon region and the eastern seas of the Philippines, where tropical cyclones were observed. Enhanced convection continued over the maritime continent near the dateline, with tropical cyclone activity (typhoons) from this enhanced convection impacting the South China Sea. From mid to late August, enhanced monsoon activity was observed from northern Southeast Asia through the South China Sea to Korea.

Figure 9 shows the infrared radiation temperature (K) and 200 hPa velocity potential (10^6 m^2/s) anomalies on August 18, 26, and September 1, 2018. Regions with high infrared radiation temperatures (brown contours) indicate low-level

clouds or dry areas unfavorable for precipitation, while regions with low infrared radiation temperatures (green contours) indicate cumulonimbus clouds favorable for precipitation. Examining the velocity potential anomaly distribution in these areas reveals that positive anomalies (blue) near the equator align with green contours or boundaries over time. This indicates that positive velocity potential anomalies near the equator, distributed towards mid-latitudes, signify the divergence of giant cumulonimbus clouds, serving as indicators for the location of typhoons, cyclones, or hurricanes near the ocean or adjacent regions, indicating favorable conditions for precipitation. In August 2018, strong Indian-Southeast Asian monsoon activity and enhanced convection (tropical cyclone or typhoon activity) continued to dominate the southeastern pattern of Asia. Korea was initially affected by tropical cyclones from the west, originating from the ITCZ in the South China Sea, followed by those in the longitude band passing through Korea, and finally those from further east, influencing the region.

Figure 10 shows the spatial distribution of the average SST anomalies across global seas from August 5 to September 1, 2018. Yellow/red and blue shading represent positive and negative anomalies, respectively. Figure 11 illustrates the weekly SST anomalies in the Pacific region on August 8, 15, 22, and 29 during this period. From August 5 to 21, SST showed negative anomalies near Indonesia and strengthened positive anomalies near the northwest Pacific at latitude 10°N. Tropical cyclones in the western Pacific formed in the tropical convergence zones of negative anomaly regions, as seen in the 200 hPa velocity potential in Figure 8. When negative anomaly areas in the western Pacific strengthened, tropical cyclones developed, whereas when positive anomaly areas to the east strengthened, western tropical cyclones moved westward, northward, or northwestward, affecting the Korean Peninsula. From August 22 to 28, SST in the western Pacific tropical convergence zone again showed strengthened negative anomalies, leading to the development of tropical cyclones. From August 29 to September 4, these tropical cyclones impacted the Korean Peninsula. Consequently, the positive SST anomalies around the Korean Peninsula in Figure 9 can be attributed to the transport of high energy from the south through typhoons or low-level jets. Therefore, while monthly and weekly SST anomaly distributions can be used to detail the formation regions of tropical cyclones, this is beyond the scope of the current study and is thus omitted.

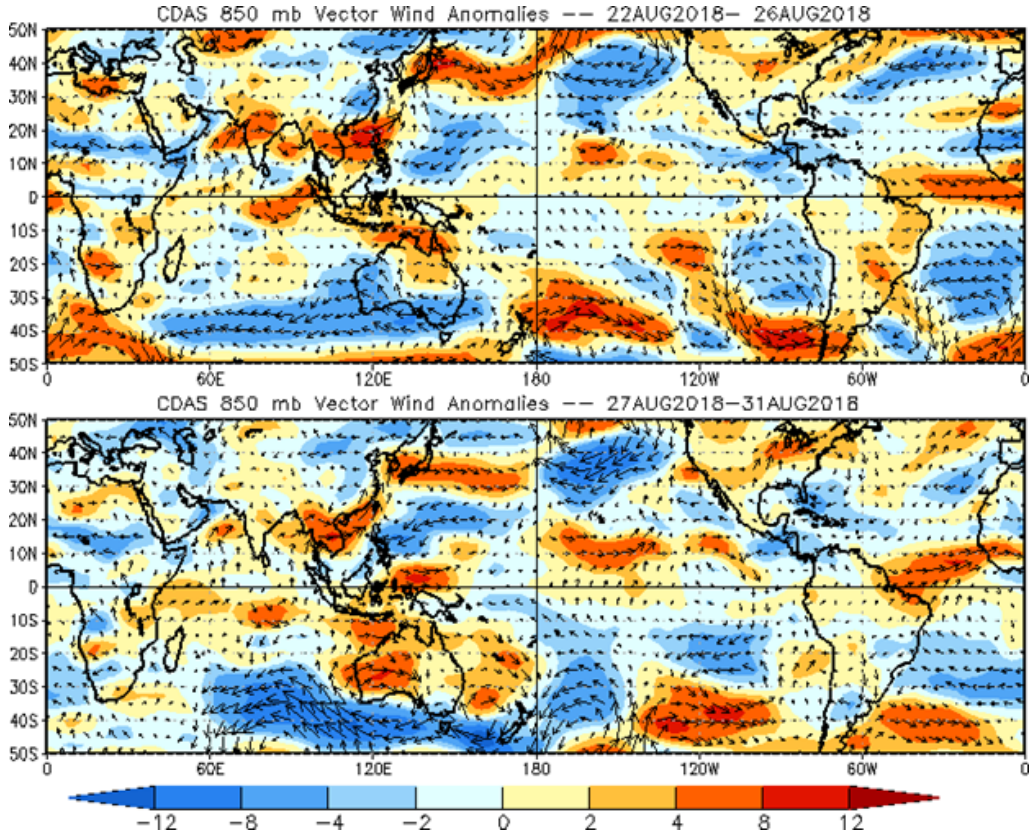

Figure 7. CDAS(Climate Data Asimilation System) 850 hPa(mb) vector wind anormalies for the period from 22 to 31 August 2018. Red and blue shades show westly and eastly, respectively.

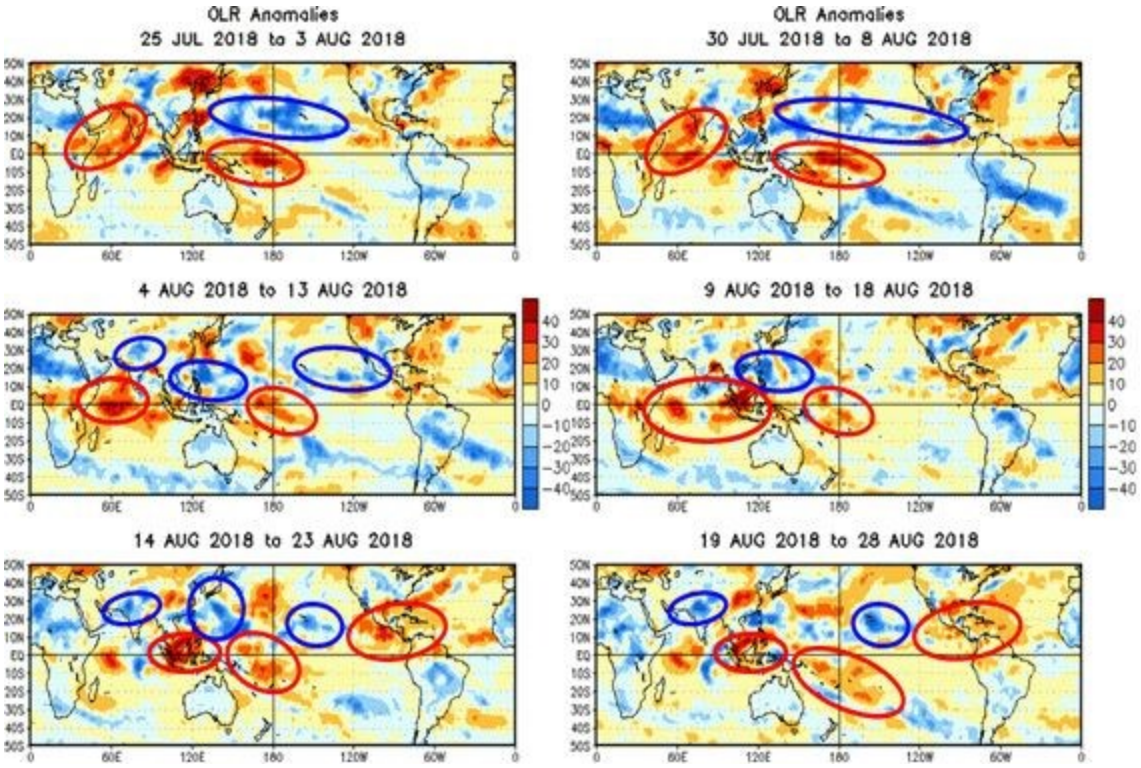

Figure 8. OLR(Outgoing Longwave Radiation) anormalies for the period from 25 July to 28 August 2018. Blue circles and shading show wetter than normal conditions, negative OLR anomalies, and red circles and shades present drier than normal conditions, positive OLR anomalies

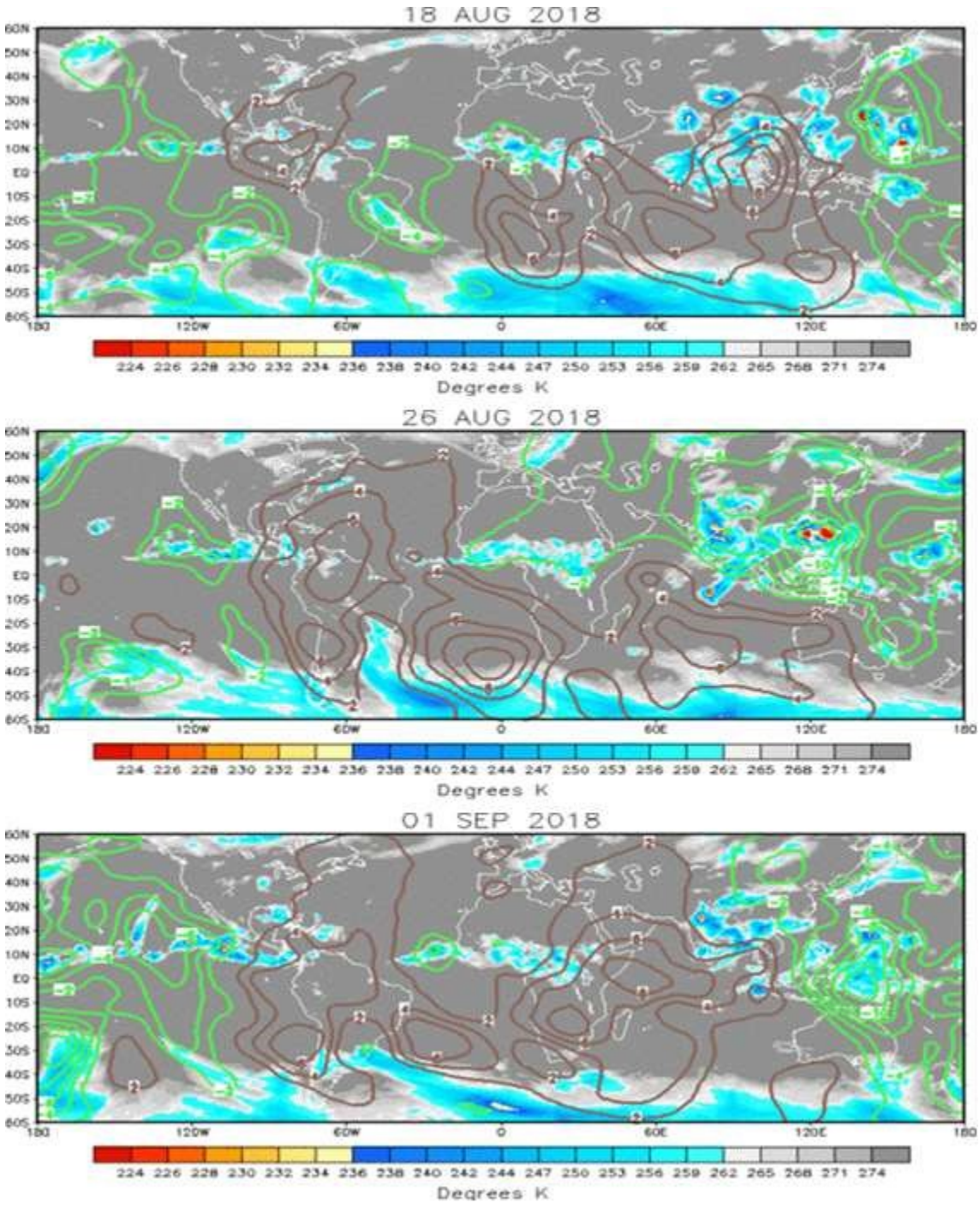

Figure 9. Infrared radiation temperatures (K) and 200hPa velocity potential anomalies($10^6 m^2 s^{-1}$) on 18 August 2018, 26 August 2018, and 1 September 2018. Positive(brown contours) and negative(green contours) anomalies indicate unfavorable and favorable conditions, respectively, for precipitation.

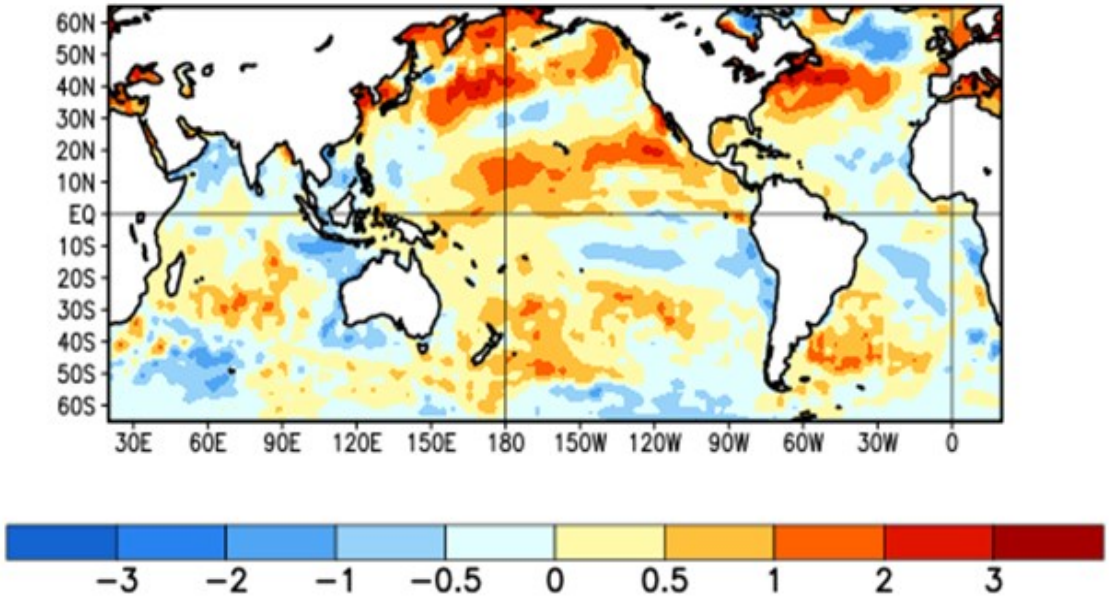

Figure 10. Spatial distribution of average SST(Sea Surface Temperature, ℃) anormalies in the global sea area for the period from 5 August to 1 September 2018. Yellow/red and blue shading shows positive and negative, respectively.

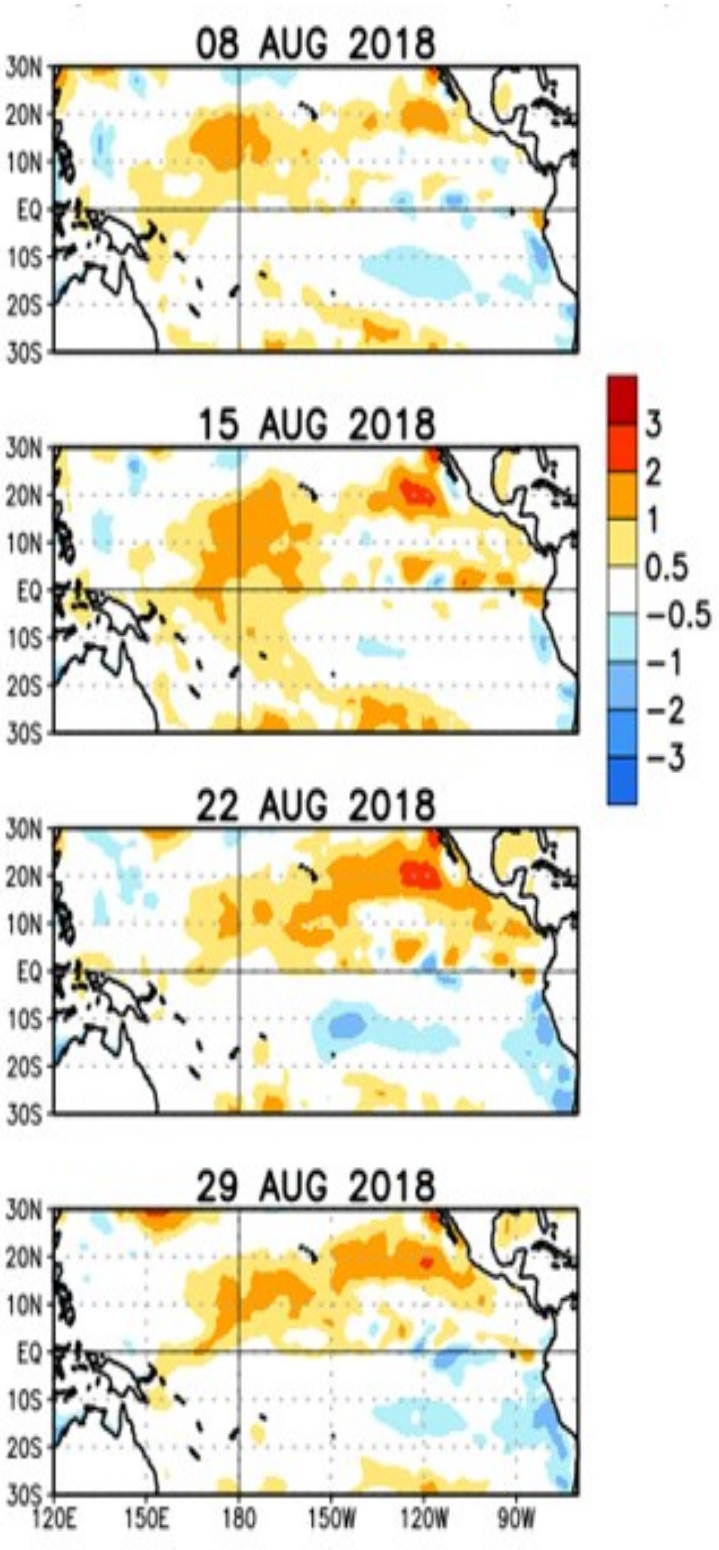

Figure 11. Spatial distribution of weekly SST(Sea Surface Temperature) anormalies(℃) in the Pacific area for the period from 8 August to 4 September 2018. Yellow/red and blue shading shows positive and negative, respectively.

4. Tracking AR Using IWV and IVT

Figures 12 shows the global distribution of TPW on September 25 and 27, 2019. It illustrates how the single large AR that passed through the Korean Peninsula on September 21, 2019 (as shown in Figure 3), split into two and affected Russia and North America four days later. Two days after that, these ARs merged back into one.

In this study, the spatial distribution of IWV above 20 mm and IVT above 250 kg/m/s was estimated using analysis data from the NCEP GFS weather model. The results are shown in Figures 13 and 14. It was confirmed that IWV closely matched the observed TPW values. Moreover, the IVT above 250 kg/m/s allowed for easy identification of the AR's movement direction and intensity.

Therefore, accurately forecasting the potential for heavy rainfall and precipitation amounts due to ARs is crucial in weather prediction. It is necessary to predict and present IWV values above 20 mm and wind fields at 850 hPa or IVT values above 250 kg/m/s.

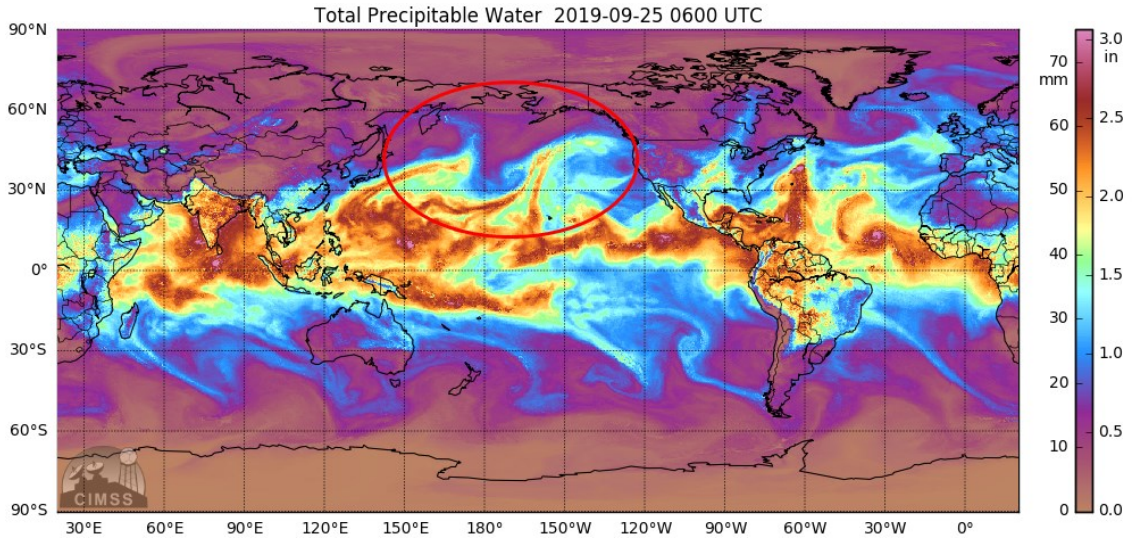

Figure 12. Spatial distribution of total precipitable water(㎜) at 0600UTC on 25 September 2019.

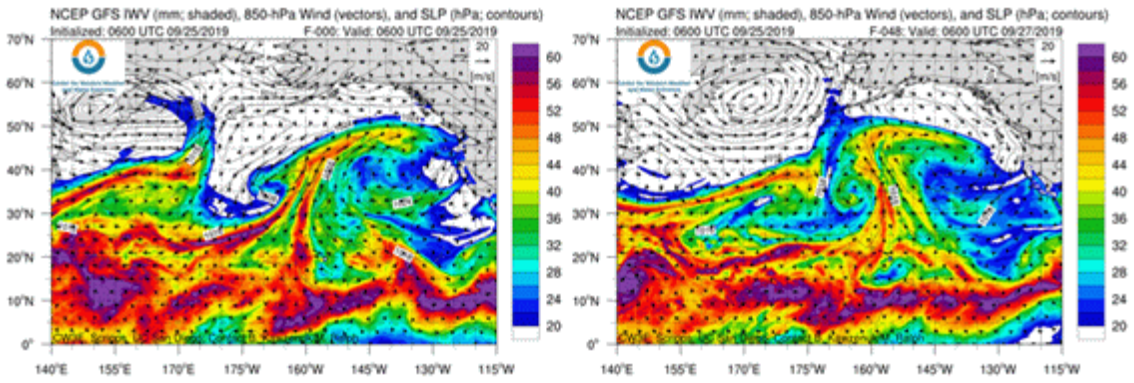

Figure 13. IWV(Integrated Water Vapour, mm) and 850hPa wind vectors in the Pacific area at 0000UTC on 25 and 27 September 2019. Color shading shows more than 20mm of IWV.

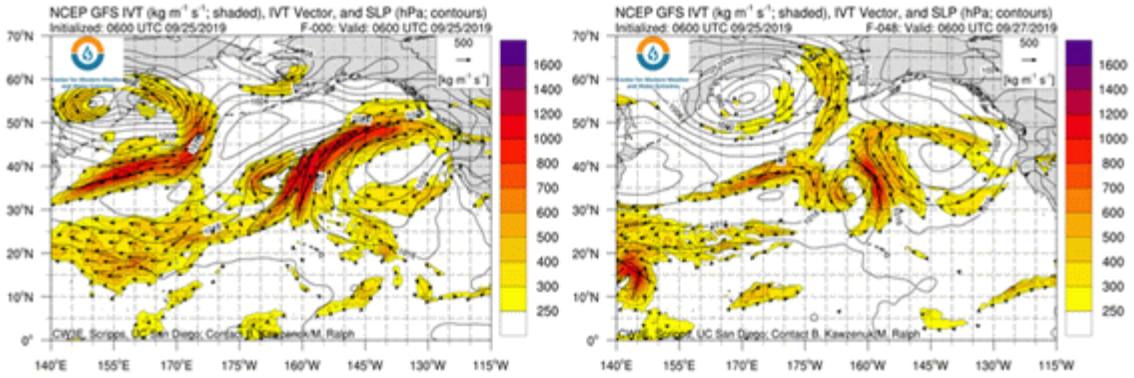

Figure 14. IVT(Integrated Vapour Transport, $kgm^{-1}s^{-1}$), IVT vector, and 850 hPa geopotential heights(m) in the Pacific area at 0000UTC on 25 and 27 September 2019. Color shading shows more than 250$kgm^{-1}s^{-1}$ of IWV.

IV. Conclusion

The purpose of this study is to understand the characteristics of heavy rainfall events that occurred during the summer on the Korean Peninsula by examining the patterns of TPW related to ARs, low-level jets, typhoons, the MJO, the ENSO, and monsoons in 2018 and 2019. Temporal variations in TPW were analyzed using data from the AMSU and SSMI satellites. Additionally, radar composite data from the Korea Meteorological Administration was used to track the transport of TPW associated with summer heavy rainfall events.

The study also analyzed the spatial distribution of ARs and their related factors, such as low-level jets, MJO, ENSO, and monsoons, using wind fields at 10m from the Korea Meteorological Administration, 850 hPa wind vector anomalies, streamlines and mixing ratio distributions from the Korea Meteorological Administration and the NOAA, OLR anomalies, SST, IWV, and IVT. The position of typhoons and the rainfall regions of the Asian summer monsoon were identified using 200 hPa velocity potential anomaly distributions and infrared radiation temperature.

The results are summarized as follows:

ARs were found to influence the flow of water vapor over the Korean Peninsula and directly impact summer heavy rainfall events, forming a band-shaped flow with TPW exceeding 20 mm along the thermal equator (or the ITCZ) extending to mid-latitudes. Specifically, the formation of tropical cyclones or typhoons near the thermal equator concentrated water vapor in the western Pacific, linking with mid-latitude cyclones towards East Asia, forming ARs or moving as typhoons, affecting precipitation. ARs and typhoons impacting the Korean Peninsula subsequently influenced North America as part of a large AR following mid-latitude cyclone fronts. The spatial distribution of TPW concentrated in high heat capacity regions during summer was found to be related to monsoons, MJO, and ENSO.

The formation regions of typhoons were identified not only using meteorological satellite images and surface weather maps but also by locating TPW nuclei exceeding 70 mm and positive (divergent) velocity potential anomalies at the 200 hPa level. The case studies from August 21-22, 2019, and August 24-27 and September 2-3, 2018, showed that these typhoons formed in areas where the monsoon trough moved northward to the northern tip of the Indochina Peninsula and connected with the ITCZ east of the Philippines. TPW was transported in a band shape along fronts where cold northern air met warm southern air in wind vector fields at an altitude of 10 km or along the strong boundary lines in the mixing ratio distribution at 850 hPa, driven by strong winds or low-level jets towards the center of comma-shaped mid-latitude cyclones. Subsequently, this band either redeveloped or was distributed by the movement of the typhoon.

Analyzing the 850 hPa wind vectors from August 22-31, 2018, revealed that during this period, when the MJO's convective region was located in the Indian monsoon region, positive anomalies (westerlies) propagated as Rossby waves from the Indian monsoon region through the Philippines, the South China Sea, Korea, Japan, to North America, with TPW distributed along these bands. OLR anomalies from late July to mid-August 2018 showed negative anomalies (indicating wet conditions or enhanced convection) concentrated from the thermal equator near the western Pacific to the Indian Southeast Asian monsoon region and the eastern seas of the Philippines, inducing the formation of tropical cyclones. From mid to late August, these enhanced convection areas extended from the South China Sea to the Korean Peninsula.

The analysis of infrared radiation temperature and 200 hPa velocity potential during this period in August 2018 also indicated dominant strong Indian Southeast Asian monsoon activity and tropical cyclone (or typhoon) activity. TPW transported to the Korean Peninsula was affected first by tropical cyclones from the east longitudinal band passing through the western sea, second by tropical cyclones from the longitudinal band passing through the Korean Peninsula, and third by tropical cyclones from further east longitudinal bands.

The analysis of average SST anomalies from August 5 to September 1, 2018, revealed that strengthened negative anomaly areas in the western Pacific tropical convergence zone led to the formation of tropical cyclones. Conversely, strengthened positive anomaly areas to the east resulted in western tropical cyclones moving westward, northward, or northwestward, impacting the Korean Peninsula with positive anomalies.

Using analysis data from the NCEP GFS weather model, the spatial distribution of IWV above 20 mm and IVT above 250 kg/m/s was estimated, and it was found that IWV closely matched observed TPW values. IVT effectively indicated the movement direction and intensity of ARs. Thus, accurately predicting IWV and IVT based on TPW and wind fields is crucial for forecasting heavy rainfall and precipitation.

Acknowledgements

This research was supported by the National Research Foundation of Korea (NRF) grant funded by the Ministry of Education of the Republic of Korea in 2018. We express our sincere gratitude for their support (No. 2018R1D1A1B07049803).

References

An, S. I., Kug, J. S., Ham, Y. G., & Kang, I. S. (2015). The impact of El Niño on the East Asian monsoon: A statistical study. *Climate Dynamics, 45*(3-4), 697-706.

Bao, J. W., Michelson, S. A., Neiman, P. J., Ralph, F. M., & Wilczak, J. M. (2006). Interpretation of enhanced integrated water vapor bands associated with extratropical cyclones: Their formation and connection to tropical moisture. *Monthly Weather Review, 134*(4), 1063-1080. doi:10.1175/MWR3123.1

Chen, G. T. J., & Yu, C. C. (1988). Study of low-level jet and extremely heavy rainfall over northern Taiwan in the Mei-Yu season. *Monthly Weather Review, 116*(5), 884-891.

Dacre, H. F., & Gray, S. L. (2015). Quantifying the climatological relationship between extratropical cyclone intensity and atmospheric river intensity. *Geophysical Research Letters, 42*(3), 944-951.

Deser, C. M., Alexander, A., Xie, S. P., & Philips, A. S. (2010). Sea surface temperature variability: Patterns and mechanisms. *Annual Review of Marine Sciences, 2*, 29-77.

Gimeno, L., Stohl, A., Trigo, R. M., Dominguez, F., Yoshimura, K., Yu, L., ... & Nieto, R. (2014). Oceanic and terrestrial sources of continental precipitation. *Reviews of Geophysics, 52*(4), 343-370.

Gimeno, L., Nieto, R., Váazquez, M., & Lavers, D. A. (2014). Atmospheric rivers: A mini-review. *Frontiers in Earth Science, 2*, 1-6. doi:10.3389/feart.2014.00002

Higgins, W., & Shi, W. (2001). Intercomparison of the principal modes of interannual and intraseasonal variability of the North American monsoon system. *Journal of Climate, 14*(3), 403-417.

Kim, H. J., Kim, D. B., Jeong, O. J., & Moon, Y. S. (2021). The moving speed of typhoons and changes in total precipitable water vapor around the Korean Peninsula. *Journal of the Korean Earth Science Society, 42*(4), 264-277.

Kim, H. K., & Seo, K. H. (2016). Cluster analysis of tropical cyclone tracks over the western North Pacific using a self-organizing map. *Journal of Climate, 29*(10), 3731-3751.

Kim, H. S. (2011). Diagnosis and prediction of the summer tropical cyclone track patterns over the western North Pacific (Ph.D. thesis). Seoul National University, Seoul, South Korea.

Kim, J., Park, R. J., Ho, C. H., Woo, J. H., Choi, K. C., Song, C. H., & Lee, H. J. (2016). Elevated aerosol layer over the Asian summer monsoon region. *Atmospheric Chemistry and Physics, 16*(2), 7361-7376.

Kim, J., Seo, K. H., & Son, S. W. (2021). The influence of tropical cyclones on the East Asian monsoon and precipitation. *Journal of Climate, 34*(7), 2845-2863.

Kim, J. H., Ho, C. H., Kim, H. S., Sui, C. H., & Park, S. K. (2008). Systematic variation of summertime tropical cyclone activity in the western North Pacific in relation to the Madden-Julian Oscillation. *Journal of Climate, 21*(5), 1171-1191.

Lee, W. J. (2006). Weather chart and weather interpretation. Ghanggyeo-etecs, 49-97.

Moon, H., Kim, J., Guan, B., Waliser, D. E., Choi, J., Goo, T. Y., ... & Byun, Y. H. (2019). The effects of atmospheric river landfalls on precipitation and temperature in Korea. *Atmosphere, 29*(4), 343-353.

Neiman, P. J., Ralph, F. M., Wick, G. A., Lundquist, J. D., & Dettinger, M. D. (2008). Meteorological characteristics and overland precipitation impacts of atmospheric rivers affecting the West Coast of North America based on eight years of SSM/I satellite observations. *Journal of Hydrometeorology, 9*(1), 22-47.

Park, C. H., Lee, H. W., & Jung, W. S. (2003). The Effects of Low-Level Jet and Topography on Heavy Rainfall near Mt. Jirisan. *Asia-Pacific Journal of Atmospheric Sciences, 39*(4), 441-458.

Seo, K. H., Choi, W., & Kim, S. (2017). The relationship between cold wakes and typhoon intensity. *Journal of Climate, 30*(2), 743-758.

Wang, B., & Lin, H. (2002). Rainy season of the Asian-Pacific summer monsoon. *Journal of Climate, 15*(4), 386-398.

Wang, B., Clemons, S. C., & Liu, P. (2003). Contrasting the Indian and east Asian monsoon: Implications on geologic timescales. *Marine Geology, 201*(1-2), 5-21.

Xie, S. P., & Hu, K. (2009). Indian Ocean capacitor effect on Indo-western Pacific climate. *Journal of Climate, 22*(10), 2802-2817.

Zhu, Y., & Newell, R. E. (1994). Atmospheric rivers and bombs. *Geophysical Research Letters, 21*(18), 1999-2002.